SEMINAR
ON
FINITE ELEMENT ANALYSIS OF REINFORCED CONCRETE STRUCTURES

Tokyo, May 21-24, 1985

Volume 1

JAPAN SOCIETY FOR THE PROMOTION OF SCIENCE

NATIONAL SCIENCE FOUNDATION

Fracture Mechanics and Strain-Softening of Concrete

Zdeněk P. Bažant

SYNOPSIS

Finite element analysis of failure of certain types of concrete structures requires modeling of distributed cracking. Propagation of failure zones with distributed cracking must be treated from the viewpoint of fracture mechanics if the calculation should be objective and properly converge as the mesh is refined. After a brief review of the crack band model, the lecture expounds a novel approach to strain-softening -- a nonlocal formulation, in which stress at a point depends on the entire strain field from a neighborhood of the point. Application of the theory is demonstrated by finite element anlaysis of waves in strain-softening materials. Finally, the formulation of strain-softening constitutive relations on the basis of the microplane model is briefly outlined, and the size effect is discussed.

Z. P. Bažant is Professor of Civil Engineering and Director of Center for Concrete and Geomaterials at Northwestern University, Evanston, Illinois 60201, U.S.A. Born in Prague, he received his Civil Eng. degree from Czech Technical University, Prague (1960) and his Ph.D. in Engineering Mechanics from Czechoslovak Academy of Sciences (1963). Currently he is Chairman of RILEM creep committee and Coordinator of SMiRT Division H, and has served as chairmen or member of various commitees in ASCE, ACI, ASME, and ASTM. He is a Registered Structural Engineer in Illinois and Consultant to Argonne National Laboratory and other firms. His works on inelastic behavior, fracture, creep, thermal effects and stability were recognized by Guggenheim and Ford Foundation fellowships, ASCE Huber Prize and Lin Award, RILEM Medal, IR-100 Award and elections as Fellow of American Academy of Mechanics and of ACI.

1. INTRODUCTION

Heterogeneous brittle materials such as concretes or rocks fail by progressive fracturing distributed over a finite-size zone within the material. In the continuum approximation, this zone is characterized by strain-softening, i.e., a stress-strain relation in which the maximum principal stress decreases at increasing strain. The purpose of the present lecture is to present an overview of some recent results obtained at Northwestern University in the use of strain-softening material models for the description of fracture propagation in concrete structures.

2. CRACK BAND MODEL

Due to the distributed nature of microcracking, as well as the fact that the path of a final crack is generally not smooth but highly tortuous, it is not unrealistic to model cracking by means of stress-strain relations, introducing strain-softening in which the major principal tensile stress is reduced to zero (Fig. 1). This approach is particularly convenient for finite element analysis, since it necessitates merely an adjustment in the incremental stiffness matrix of the finite element.

In the form of sudden cracking, this approach was introduced in 1967 by Rashid [27,19]. For strain-softening analysis of fracture this approach was developed in Ref. 4-5, in which the strain-softening triaxial stress-strain relation was introduced in the form.

$$\underset{\sim}{\varepsilon} = \underset{\sim}{D}\underset{\sim}{\sigma} + \underset{\sim}{\xi} \tag{1}$$

Here $\underset{\sim}{\varepsilon}$ and $\underset{\sim}{\sigma}$ are the column matrices of the components of strain and stress, $\underset{\sim}{D}$ is the 6 x 6 matrix of elastic constants, and $\underset{\sim}{\xi} = (\xi_{11}, \xi_{22}, \xi_{33}, 0, 0, 0)^T$, where superscript T denotes a transpose and the numerical subscripts refer to cartesian coordinates $x_i (i = 1,2,3)$; ξ is the column matrix of additional smeared-out strains due to cracking. The normal stresses are assumed to be uniquely related to their associted cracking strains (Fig. 1), i.e.,

$$\sigma_{11} = C(\xi_{11})\xi_{11}, \quad \sigma_{22} = C(\xi_{22})\xi_{22}, \quad \sigma_{33} = C(\xi_{33})\xi_{33} \tag{2}$$

in which C is the secant modulus which reduces to zero at very large cracking strain and may be calibrated from direct tensile test data [21,22,23,24,27,28]. Different algebraic relations are used for unloading. In this formulation it is assumed that cracking can occur only in three mutually orthogonal directions which are known in advance and do not rotate against the material once the cracking starts.

In the classical formulation of finite element analysis of concrete structures, as employed in the current large computer programs, a strain-softening stress-strain relation, mostly one that exhibits a sudden stress drop, is used indiscriminately for an arbitrarily chosen finite element size. It has been demonstrated, however, that this approach is inconsistent, unobjective with regard to the analyst's choice of the element size. It can yield greatly different results for different mesh sizes and converges to a physically meaningless solution as the mesh size is refined to zero [3,7-9]. For failures of the brittle type, the load causing further fracture extension converges to zero as the mesh size tends to zero. So does the total energy consumed by failure of the structure, which is an unrealistic result.

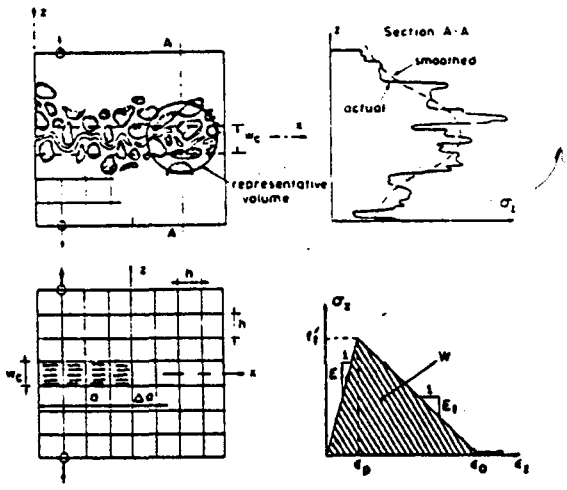

Fig. 1 Fracture in a heterogeneous aggregate material, statistical scatter of stress, crack band model, and strain-softening stress strain diagram

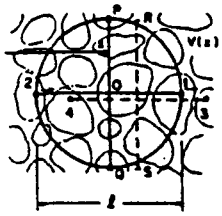

Fig. 2 Characteristic volume of a heterogeneous material

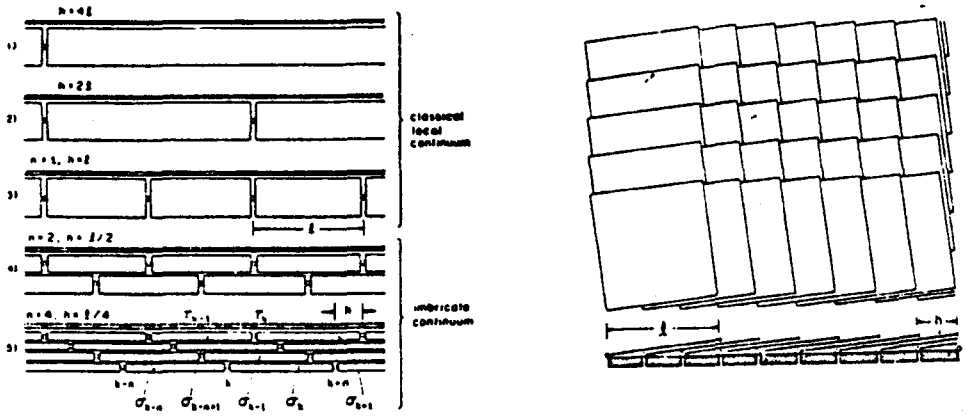

Fig. 3 Illustration of mesh refinement for a one dimensional imbricate continuum (left) and of element arrangement for a two-dimensional imbricate continuum (right) (the elements are slightly rotated for the purpose of illustration)

It has been shown that these incorrect features can be eliminated by using an energy criterion rather than the stress-strain relation as the primary condition for the extension of the cracked band of finite elements. Considering a crack band of a single-element width, consisting of finite elements with a uniform strain distribution across the band, the fracture energy, i.e., the energy consumed per unit extension of the crack band (and per unit thickness), may be expressed as

$$G_f = w_c \int \sigma_{33}\, d\varepsilon_{33} = \frac{w_c}{2}\, f'^2_t \left(\frac{1}{E_0} - \frac{1}{E_t} \right) \qquad (3)$$

in which w_c is the width of the crack band front, which must be considered as a material property [3], σ_{33} is the normal stress across the central plane of the crack band, f'_t if the direct tensile strength of the material, E_0 is the initial elastic Young's modulus, and E_t is the mean downward slope of the strain-softening segment of the stress-strain diagram, which is negative.

It was found that if w_c is taken as roughly 3-times the maximum aggregate size in concrete [5], then the crack-band finite element yields results which agree with all essential experimental evidence from fracture tests, both the maximum load data and the R-curves [20,29]. However, since the cracking at the failure front always tends to localize into a single-element width, the use of the correct element size $h = w_c$ is essential. For large structures, such elements are impracticably small, and a larger element size needs to be used. It was shown [7-9,5] that this leads to consistent results if the value of fracture energy G_f is preserved. This can be achieved by adjusting the value of E_t, or f'_t, or both, in Eq. 3 in which w_c is replaced by h. So, one must use some equivalent strain-softening slope and some equivalent tensile strength, depending on the element size, if consistent results should be achieved.

On the other hand, one may imagine the width of the crack band to be reduced to zero, and if the strain-softening slope E_t is adjusted so as to keep the correct value of G_f, the model in the limit becomes equivalent to the use of the stress-displacement relation on the centerline of fracture. This limiting case of the crack band model coincides with the model of Hillerborg et al. [11,21].

The adjustment of constitutive properties in order to achieve consistent results for different mesh sizes is, however, disconcerting from the fundamental, mathematical viewpoint. It appears as if the finite element model was approximating a continuum that is not uniquely defined. Obviously, in the crack band model we cannot say we are approximating the solution for a classical, local continuum because for such a continuum the crack band can, of course, localize into a layer of zero thickness, while an adjustment of material properties is not permitted.

The source of the difficulty appears to be [1,2] the assumption that we deal with a local continuum, in which the stress at a certain point is a function of the strain at the same point. We now focus attention to the development of a new type of continuum for which the aforementioned mathematical difficulties do not arise. At the same time we gain with this new type of continuum a means to resolve in detail the distributions of averaged stress and strain throughout the failure zone.

3. NONLOCAL CONTINUUM APPROACH

From the works of Kröner and others [12-16], it is known that in a statistically heterogeneous medium which is not in a macroscopically homogeneous state of strain, the averaged (smoothed) stress at a certain point depends not only on the gradient of the averaged displacements at that same point (local properties), but also on the averaged displacements within a certain characteristic finite neighborhood of that point. The properties of such a medium cannot, therefore, be said to be local, and the medium is called nonlocal.

The nonlocal displacement gradient may be defined by the relation

$$D_i u_j(\underset{\sim}{x}) = \frac{1}{V}\int_{V(\underset{\sim}{x})} \frac{\partial u_j(\underset{\sim}{x}')}{\partial x_i}\, dV' = \frac{1}{V}\int_{S(\underset{\sim}{x})} u_j(\underset{\sim}{x}')\, n_i(\underset{\sim}{x}')\, dS' \qquad (4)$$

in which u_j are the cartesian displacement components ($j = 1, 2, 3$), $\underset{\sim}{x}$ is the coordinate vector of the given point characterized by cartesian coordinates x_j, $V(\underset{\sim}{x})$ is the characteristic volume of the material (Fig. 2) centered at point $\underset{\sim}{x}$ (Fig. 2), $S(\underset{\sim}{x})$ is the surface of this volume, $n_i(\underset{\sim}{x}')$ is the unit normal of this surface at point $\underset{\sim}{x}'$, and D_i is the gradient averaging operator. The surface integral in Eq. 4 follows from the volume integral by application of the Gauss integral theorem. More generally, a weighting function can be introduced in Eq. 4. Using the gradient averaging operator, the mean strains may be defined as

$$\bar{\varepsilon}_{ij} = \frac{1}{2}(D_i u_j + D_j u_i) \qquad (5)$$

In previous works dealing with nonlocal continua it has been generally assumed that the continuum equation of motion may be written as

$$\frac{\partial}{\partial x_j}\bar{C}_{ijkm}(\underset{\sim}{\bar{\varepsilon}})\, D_m u_k = \rho \ddot{u}_i \qquad (6)$$

in which C_{ijkm} are secant elastic moduli which, in general, depend on the mean strain, ρ is the mass density, and superior dots refer to time derivatives. It is found, however, that Eq. 3 is incapable of describing a strain-softening continuum. It always leads to unstable response as soon as strain-softening begins. The difficulty has been traced to the asymmetry of these equations due to the combination of partial derivatives $\partial/\partial x_j$ with the gradient averaging operator D_m. This nonsymmetry gives rise to nonsymmetric finite element matrices even if C_{ijkm} are constant, i.e., if the medium is elastic. Such a nonsymmetry is certainly an objectional property.

For this reason, a systematic derivation of the continuum equation of motion on the basis of Eq. 4 has been attempted, using the calculus of variations. It has been found [2, 25] that the proper form of the continuum equation of motion is

$$(1-\gamma)D_j\bar{C}_{ijkm}(\underset{\sim}{\bar{\varepsilon}})D_m u_k + \gamma\frac{\partial}{\partial x_j}C_{ijkm}(\underset{\sim}{\varepsilon})\frac{\partial}{\partial x_m}u_k = \rho\ddot{u}_i \qquad (7)$$

in which γ is an empirical coefficient between 0 and 1, and C_{ijkm} are the loca secant moduli. In contrast to Eq. 6, each term of the last equation has a symmetric structure, and consequently, discretization by finite elements leads to symmetric stiffness matrices if the elastic moduli $\bar{C}_{ijkm}$ and C_{ijkm} are symmetric.

Eq. 4 can also be written in the form

$$(1-\gamma)D_j\sigma_{ij} + \gamma\,\tau_{ij,j} = \rho\,\ddot{u}_i \tag{8}$$

in which

$$\sigma_{ij} = \bar{C}_{ijkm}\,(\bar{\varepsilon})\,\varepsilon_{km} = \bar{C}_{ijkm}(\bar{\varepsilon})D_m u_k \tag{9}$$

$$\tau_{ij} = C_{ijkm}\,\varepsilon_{km} = C_{ijkm}\frac{\partial u_k}{\partial x_m} \tag{10}$$

τ_{ij} are the usual, local stresses, and σ_{ij} are the stresses characterizing the stress state in the entire representative volume of the material, called the broad-range stresses [1, 2].

When the continuum defined by Eq. 7 is discretized by finite elements the size of which is smaller than the size ℓ of the representative volume, one obtains a system of overlapping (or imbricated) finite elements visualized in Fig. 3. Therefore, the present type of nonlocal continuum has been called imbricate. The finite elements keep a constant size ℓ as the mesh is refined, and the number of finite elements crossing a given point is inversely proportional to the mesh size, while the cross section of these elements diminishes so that all imbricated elements have the same total cross section for any mesh size. It can also be shown that the limiting case of the finite difference equations describing such an imbricated system of finite elements is the differential equation in Eq. 4 [1]. If the finite element size h is larger than the characteristic length ℓ, then the finite element model of the imbricate continuum becomes identical to that for the classical local continuum.

To assure convergence and stability, the local stress-strain relations (Eq. 10) may not exhibit strain-softening, or else unstable response and spurious sensitivity to mesh size, along with incorrect convergence, may be obtained. The strain-softening properties must be described solely by the broad-range stress-strain relation in Eq. 9.

4. EXAMPLES: WAVES IN STRAIN-SOFTENING MATERIALS

To demonstrate that the concept of imbricate nonlocal continuum yields convergent finite element solutions for problems with a finite-size strain-softening zone, we will now describe two examples of one-dimensional waves. As the first example, Fig. 4 reproduces some of the results of explicit dynamic finite element calculations from Ref. 13, in which wave propagation in a strain-softening bar of length ℓ was analyzed. The characteristic length ℓ for nonlocal solution is assumed to be 1/5 of bar length L. Both ends of the bar are subjected to a constant outward velocity v_0 beginning at time t = 0. This loading produces step waves of strain propagating inward. When these waves meet at midlength, the strain suddenly increases and strain-softening ensues.

If this problem is analyzed with the usual finite element method for local continuum, it is found that strain-softening always localizes into a single finite element. Thus, the width of the strain-softening zone reduces to zero as the element mesh is refined. As a consequence, the energy W

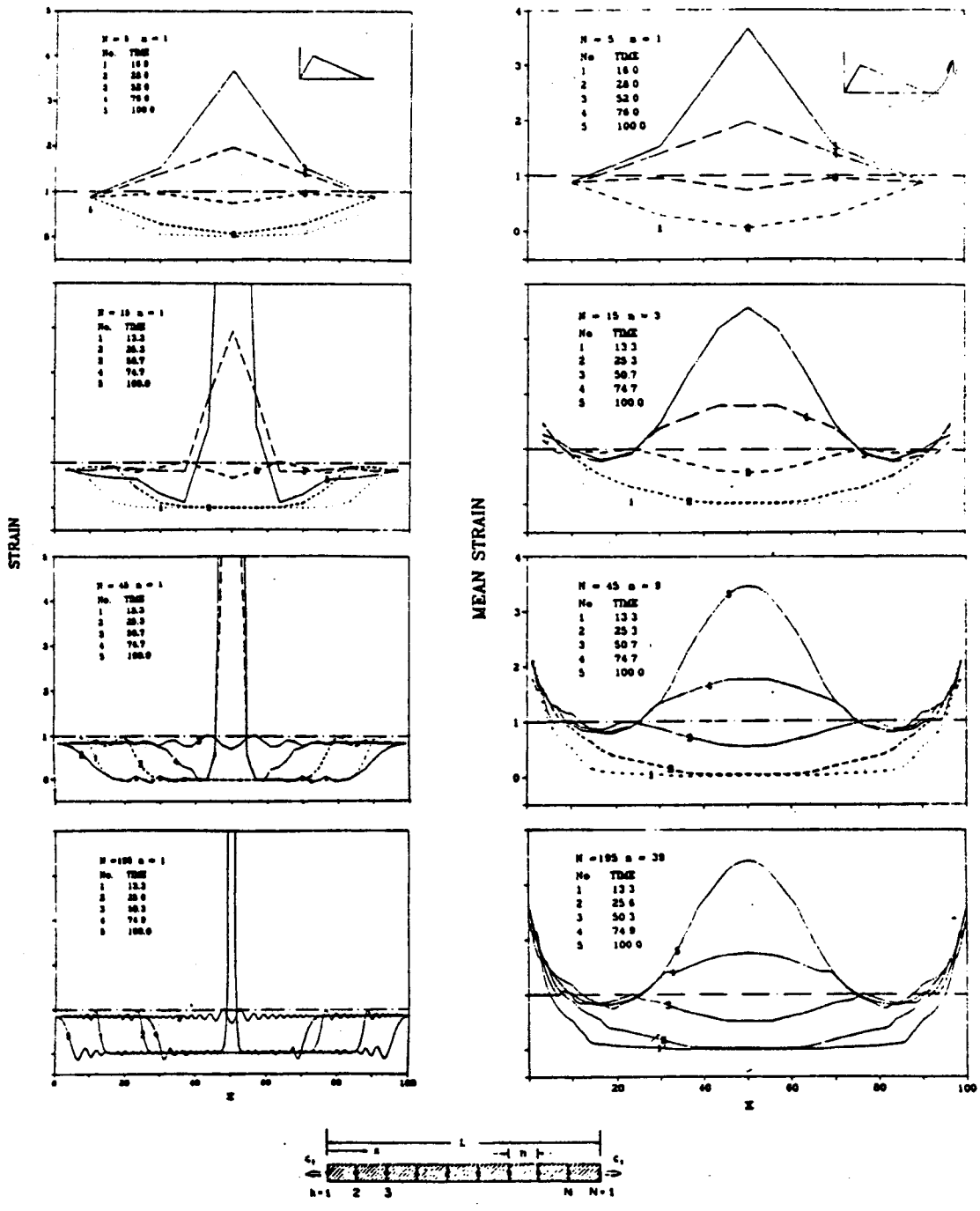

Fig. 4 Numerical results of Bažant, Chang and Belytschko [1] for wave propagation in a strain-softening bar, obtained with different numbers N of identical elements (left column - local continuum, right column - imbricate nonlocal continuum)

consumed by failure decreases with decreasing mesh size and approaches zero as the mesh size tends to zero (Fig. 5). Moreover, the finite element model of local continuum exhibits a discontinuous dependence of response on the prescribed end velocities as well as on the slope E_t of the strain-softening branch [30]. The solution, however, converges to a unique exact solution [30], although this solution is unrealistic from the physical point of view.

By contrast, for the present imbricate continuum, the solution of wave propagation in the strain-softening bar exhibits correct convergence, with a strain-softening zone of a finite size in the limit (Fig. 4, right column). Also, the energy consumed by failure in the bar converges to a finite value, as shown in Fig. 5.

As another example, we now briefly describe the solution for an implosive (converging) spherical wave which was originally described in detail in Ref. 10. Although this problem is also one-dimensional it involves three-dimensional stress and strain states. Like for the bar problem, strain-softening is produced inside the body but there is an important difference -- waves can pass through the points of strain-softening even if a local continuum is assumed.

We consider a wave generated by a sudden application of a constant uniform pressure p at the exterior surface of a hollow sphere of a hollow infinite cylinder. The pressure is a Heaviside step function of time, i.e. the boundary condition at $x = b$ (Fig. 6a) is $\sigma_x = p_0 H(t)$, and the interior surface is load-free, i.e. $\sigma_x = 0$ at $x = a$ (a, b = internal and external suface radii, x = radial coordinate). Initially, at $t = 0$, the body is at rest. The elastic solution, as is well known [31], consists of a wave with a step front of strain whose magnitude is growing as the wave front propagates toward the center. Therefore, at a certain time t_1 (and at $x = x_1$), the strain at the wavefront reaches the elastic limit, and if the material has strain-softening properties, strain-softening is thus produced in the interior of the solid, while for unaxial waves (planar wavefront) strain-softening can be produced in the interior only if waves of opposite directions meet.

The governing differential equations in spherical coordinates are:

$$\varepsilon_x = u_{,x}, \quad \varepsilon_y = \frac{u}{x}, \quad \varepsilon_z = \varepsilon_y \tag{11}$$

$$\varepsilon = \varepsilon_x + 2\varepsilon_y, \quad e_x = \frac{2}{3}(\varepsilon_x - \varepsilon_y), \quad e_y = \frac{1}{3}(\varepsilon_y - \varepsilon_x) \tag{12}$$

$\bar{\varepsilon}_x, \bar{\varepsilon}_y, \bar{\varepsilon}, \bar{e}_x, \bar{e}_y$ = the means of $\varepsilon_x, \varepsilon_y, \varepsilon, e_x, e_y$ analogous to Eq. 11 (13)

$$\sigma_{x,t} = \bar{K}\,\bar{\varepsilon}_{,t} + 2\bar{G}\,\bar{e}_{x,t}, \quad \sigma_{y,t} = \bar{K}\,\bar{\varepsilon}_{,t} + 2\bar{G}\,\bar{e}_{y,t} \tag{14}$$

$$\tau_{x,t} = K\varepsilon_{,t} + 2G\,e_{x,t}, \quad \tau_{y,t} = K\varepsilon_{,t} + 2G\,e_{y,t} \tag{15}$$

$$\bar{\sigma}_x(x) = \int_{x-1/2}^{x+1/2} \sigma_x(x+s)\,w(s)\,ds, \quad \bar{\sigma}_y(x) = \int_{x-1/2}^{x+1/2} \sigma_y(x+s)\,w(s)\,ds \tag{16}$$

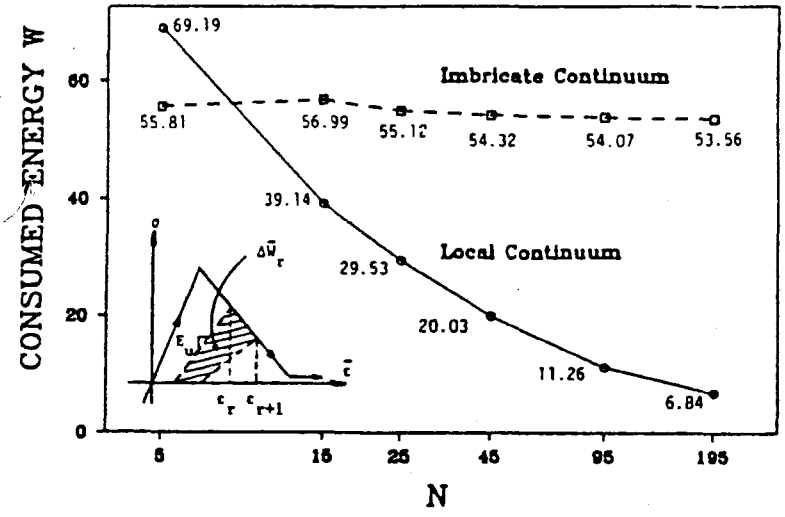

Fig. 5 Energy consumed by failure caused by wave propagation in a one-dimensional bar

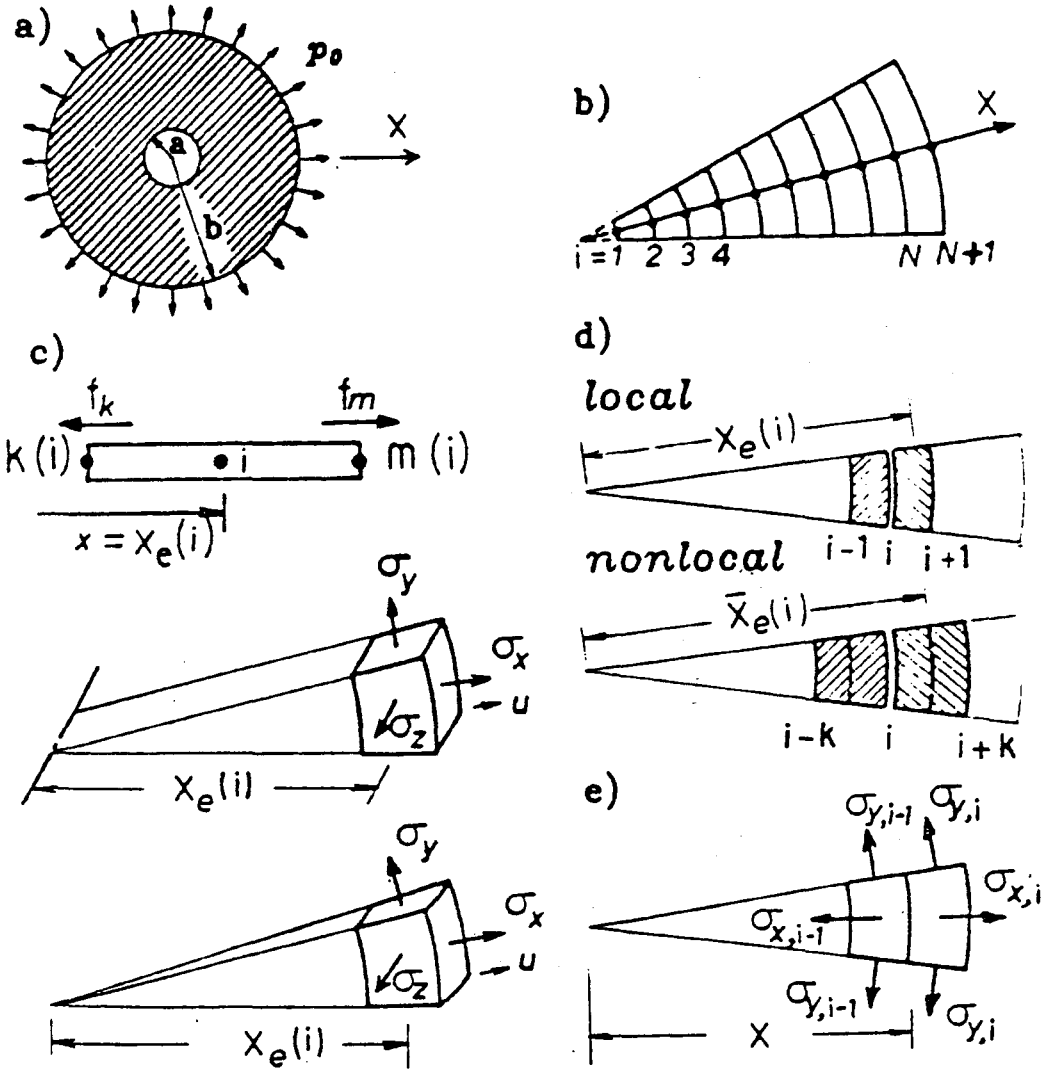

Fig. 6 Spherical waves and finite elements in spherical coordinates

$$S_x = (1-\gamma)\,\bar{\sigma}_x + \gamma\tau_x, \quad S_y = (1-\gamma)\,\bar{\sigma}_y + \gamma\tau_y \tag{17}$$

$$S_{x,x} + \frac{2}{x}(S_x - S_y) = \rho u_{,tt} \tag{18}$$

Here u = radial displacement, x = radial coordinate (Fig. 6a); ε_x, ε_y = radial and circumferential normal strains (local); ε, e_x, e_y = volumetric strain (= volume change) and deviatoric strains (local), τ_x, τ_y = local radial and circumferential normal strains; σ_x, σ_y = broad-range radial and circumferential normal stress; S_x, S_y = total radial and circumferential normal stresses, K, G, $\bar{K}$, $\bar{G}$ = local and broad-range (nonlocal) bulk and shear moduli. In Eq. (18), isotropy of the material is assumed. The shear moduli G, $\bar{G}$ are assumed to be constant, while K and $\bar{K}$ depend on ε and $\bar{\varepsilon}$, respectively; $K>0$ but $\bar{K}$ may become negative, which represents strain-softening. Eq. 18 represents the differential equations of motion of the usual form [31].

For elastic spherical wave, the present problem has a closed-form solution:

$$u = -\frac{b^3 p_o}{4Gr^2}\left\{1-e^{\xi\tau}\left[\frac{\xi}{\omega}\left(\frac{2r}{b} - 1\right)\sin\omega\tau + \cos\omega\tau\right]\right\} \qquad \text{for } \tau>0 \tag{19}$$

as may be checked by substituting in Eqs. 11-18 with $\gamma = 1$, and K = constant;

and

$$\tau = t-(b-r)/c_1, \quad \xi = 2c_2^2/(bc_1),$$

$$\omega = \xi\left[(c_1/c_2)^2 - 1\right]^{1/2}, \quad c_1 = \left[3K(1-\nu)/(1+\nu)\rho\right]^{1/2}, \tag{20}$$

$$c_2 = (G/\rho)^{1/2}, \quad \nu = (3K - 2G)/(6K + 2G)$$

For the purpose of numerical solution, a one-dimensional mesh with constant step h is used (Fig. 6b). All finite elements are two-node elements with a linear distribution of displacement u, integrated with a single numerical integration point at the element center. This is true of both the local elements of length h and the imbricate elements of length $\ell = nh$. Mass is lumped in the nodes. The radial nodal forces are referred to a radial conical segment of sphere such that its cross section area at unit distance from the center of coordinates is 1 (for the cylinder, this is the radian sector). The computational algorithm is similar to the usual explicit algorithm and is as follows.

Read a, b, ℓ, n, Δt (time step), N_e, $\bar{N}_e$, N_k, N_t (numbers of all local and imbricate elements, of all modes and of time steps), γ, and p_0. Generate arrays $\hat{k}(i)$, $\hat{m}(i)$, $\ell_e(i)$, $x_e(i)$, $\bar{k}(i)$, $\bar{m}(i)$, $\bar{\ell}_e(i)$, $\bar{x}_e(i)$ giving the number

of the left and right nodes of the i^{th} local or imbricate element, its length, and its coordinate at the center of element. Also generate externally applied nodal forces for $f^{ext}_{k,r}$. Initialize as zero the values (for r = 1) of $v_{k,r}$,

$m_{k,r}$, $\tau_{xk,r}$, $\tau_{yk,r}$, $\sigma_{yk,r}$, $\max \varepsilon_k$, $\max \bar{\varepsilon}_k$, $\tau_{\max \varepsilon,k}$, $\sigma_{\max \varepsilon,k}$,

for all k=1,...N_e (local elements) and k=1,...$\bar{N}_e$ (imbricate elements).

2. DO 8, r=2,...N_t.

3. Initialize nodal forces $F_k = 0$, $f_k = 0$ (for all modes, k=1,...N_k).

4. DO 5 i=1,...N_e (local elements).

5. Set k=k(i), m=m(i), x=x_e(i), and evaluate

$\Delta\varepsilon_{xi,r} = (v_{m,r} - v_{k,r})\Delta t/h$, $\varepsilon_{xi,r} = \varepsilon_{xi,r-1} + \Delta\varepsilon_{xi,r}$, $\Delta\varepsilon_{yi,r} = (v_{m,r} + v_{k,r})\Delta t/2x$, $\varepsilon_{yi,r} = \varepsilon_{yi,r-1} + \Delta\varepsilon_{yi,r}$. For shperical wave $\Delta\varepsilon_{i,r} = \Delta\varepsilon_{xi,r} + 2\Delta\varepsilon_{yi,r}$.

Then call a subroutine which determines the incremental tangential moduli $K_{i,r}$, $G_{i,r}$ for the local elements from their strains $\varepsilon_{xi,r}$, $\varepsilon_{yi,r}$, $\varepsilon_{i,r}$ and also decides whether virgin loading, unloading or reloading applies. Then calculate

$\Delta\tau_{xi,r} = K_{i,r}\Delta\varepsilon_{i,r} + 2G_{i,r}e_{xi,r}$, $\Delta\tau_{yi,r} = K_{i,r}\Delta\varepsilon_{i,r} + 2G_{i,r}e_{yi,r}$, $\tau_{xi,r-1} + \Delta\tau_{xi,r}$, $\tau_{yi,r} = \tau_{yi,r-1} + \Delta\tau_{yi,r}$. Then calculate all the local nodal forces at element nodes k and m (Fig. 6c);

$$\Delta f_k = -\gamma[\tau_{xi,r}x^2 - \tau_{yi,r}(x - \tfrac{h}{2})h]$$
$$\Delta f_m = \gamma[\tau_{xi,r}x^2 + \tau_{yi,r}(x + \tfrac{h}{2})h] \qquad (21)$$

These forces are accumulated at each node, $f_k \leftarrow f_k + \Delta f_k$, $f_m \leftarrow f_m + \Delta f_m$.

6. DO 7, i=1,...$\bar{N}_e$ (imbricate elements).

7. Set $k = \bar{k}(i)$, $m = \bar{m}(i)$, $\ell = \bar{\ell}_e(i)$, $x = \bar{x}_e(i)$ and evaluate

$\Delta\bar{\varepsilon}_{xi,r} = (v_{m,r} - v_{k,r})\Delta t/l$, $\bar{\varepsilon}_{xi,r} = \bar{\varepsilon}_{xi,r-1} + \Delta\bar{\varepsilon}_{xi,r}$, $\Delta\bar{\varepsilon}_{yi,r} = (v_{m,r} + v_{k,r})\Delta t/2x$, $\bar{\varepsilon}_{yi,r} = \bar{\varepsilon}_{yi,r-1} + \Delta\bar{\varepsilon}_{yi,r}$. For spherical wave $\Delta\bar{\varepsilon}_{i,r} = \Delta\bar{\varepsilon}_{xi,r} + 2\Delta\bar{\varepsilon}_{y,r}$. Then call a subroutine which determines the incremental (tangential) moduli $\bar{K}_{i,r}$, $\bar{G}_{i,r}$ for the imbricate elements from their mean strains $\bar{\varepsilon}_{xi,r}$, $\bar{\varepsilon}_{yi,r}$, $\bar{\varepsilon}_{i,r}$ and also decides whether virgin

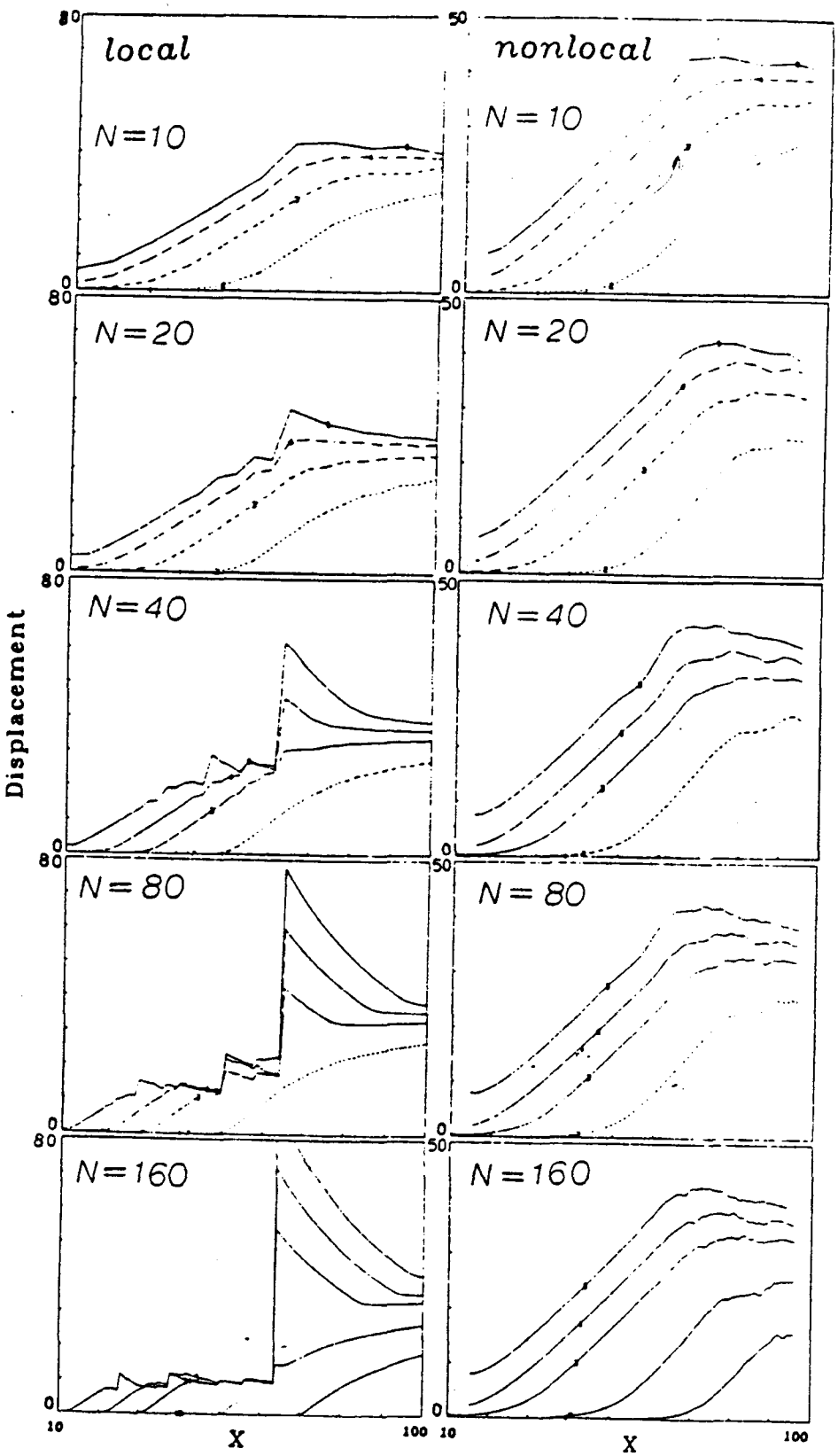

Fig. 7 Radial displacement profiles at various times obtained for various finite element subdivisions (N = number of elements)

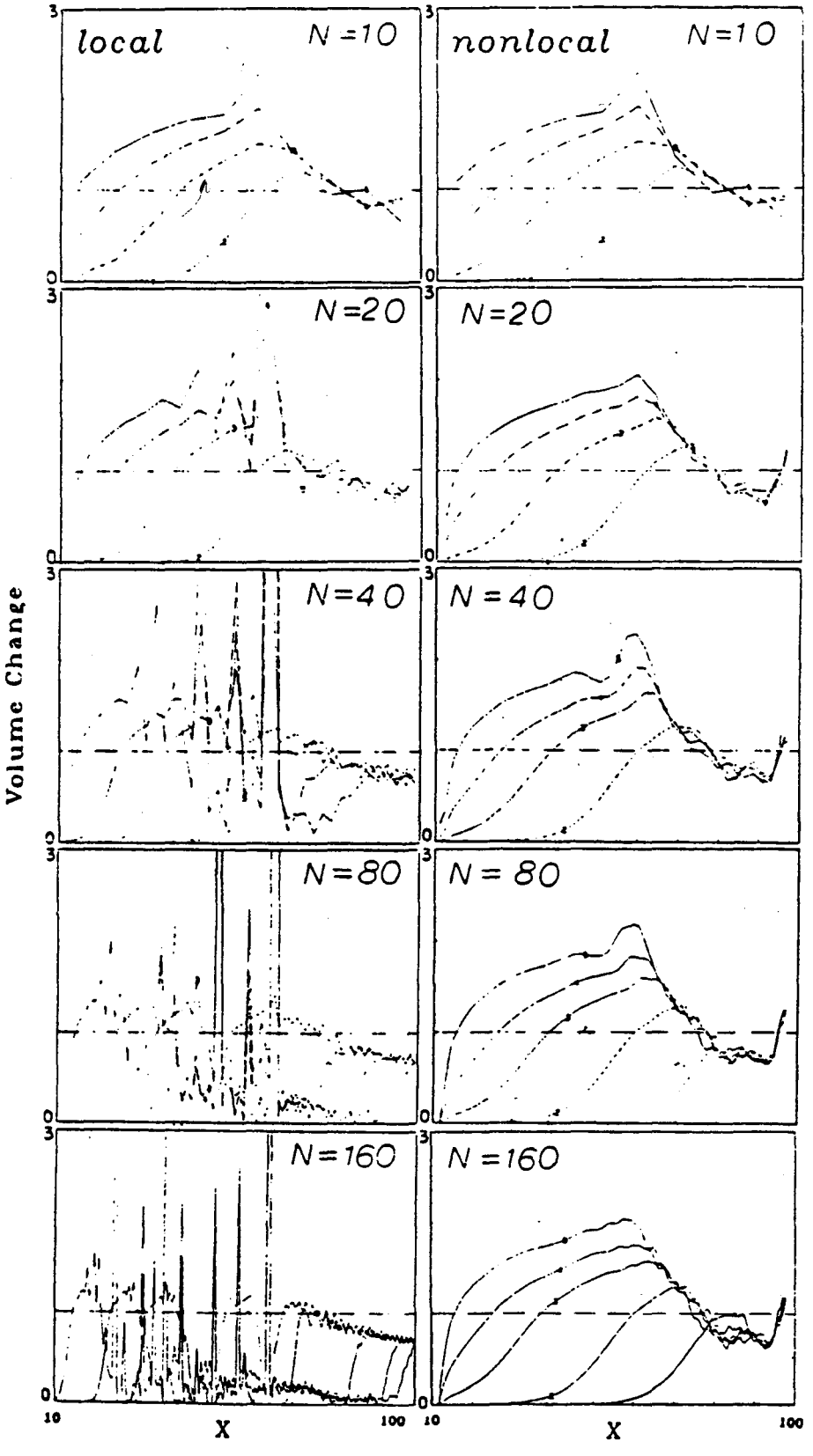

Fig. 8 Volumetric strain profiles at various times obtained for various finite element subdivisions (N = number of elements)

loading, unloading or reloading applies. Then calculate

$\Delta\sigma_{xi,r} = \bar{K}_{i,r}\,\Delta\varepsilon_{i,r} + 2\bar{G}_{i,r}\,e_{xi,r}$, $\Delta\sigma_{yi,r} = \bar{K}_{i,r}\,\Delta\varepsilon_{i,r} + 2\bar{G}_{i,r}\,e_{yi,r}$, $\sigma_{xi,r} = \sigma_{xi,r-1} + \Delta\sigma_{xi,r}$, $\sigma_{yi,r} = \sigma_{yi,r-1} + \Delta\,\sigma_{yi,r}$. Then calculate all the nonlocal nodal forces at element nodes k and m (Fig. 6d):

$$\Delta F_k = -\frac{1-\gamma}{n}\left[\sigma_{xi,r}\,x^2 - \sigma_{yi,r}\,(x-\tfrac{h}{2})h\right]$$
$$\Delta F_m = \frac{1-\gamma}{2}\left[\sigma_{xi,r}\,x^2 + \sigma_{yi,r}\,(x+\tfrac{h}{2})h\right] \qquad (22)$$

These forces are then accumulated at each node:

$F_k \leftarrow F_k + \Delta F_k$, $F_m \leftarrow F_m + \Delta F_m$.

7. DO 8, k=1,...N_k (all nodes).

8. Calculate

$v_{k,r} = v_{k,r-1} + (F_k + f_e + f^{ext}_{k,r})\Delta t/(\rho h x^2)$, $u_{k,r} = u_{k,r-1} + \Delta t\; v_{k,r}$.

For more detailed explanations, a similar algorithm for unaxial stress wave given in Ref. [1] may be consulted. It may be checked that the sum of nodal forces according to Eqs. (21) - (22) in one node yields a second-order discrete approximation of the continuum equation of motion, Eq. 18.

Figs. 7-8 show the numerical results obtained with the foregoing algorithm for the special case of volumetric strain-softening. The shear moduli G and $\bar{G}$ are assumed to be negligibly small (10^{-6}), and the bulk behavior follows the bilinear total stress-strain diagram in Fig. 11a, characterized by elastic bulk moduli $\bar{K} = \bar{K}_o = 1$, strain $\varepsilon_p = 1$ at peak stree, and $\varepsilon_f = 5$ at the end of softening. This diagram is obtained by assuming that the local behavior is elastic-ideal plastic, and that the broad-range behavior (Fig. 9a) exhibits oversoftening the purpose of which is to achieve that, for the total behavior, the strain-softening terminates at exactly zero stress [1]. The use of coefficient γ is required for stability. For one-dimensional planar waves, it was shown [7] that stability is assured for $\gamma > 0$. However, γ - values too close to 0 are not possible for numerical solutions since they lead to an ill-conditioned equation system and produce excessive noise. For one-dimensional planar waves, the value $\gamma = 0.1$ gave noise-free response. The same value sufficed for the spherical wave ($\gamma = 0.1$), in order to obtain a response with noise-free appearance. The value of the applied surface pressure is chosen as $p_0 = 0.708$. For this boundary condition, the wave propagating from the outer surface remains elastic until the wavefront reaches 30% of the thickness b-a. The dimensions are a=10, b=100, L = b-a = 90.

The nonlocal in elastic finite element program was first verified by running with it the solution for the special case of an elastic local material, for which one may set $\varepsilon_p = 10^0$, $\varepsilon_f = 10^7$, $\ell = h =$ mesh step (ℓ is variable). The convergence with increasing numbers of elements (N = 10, 20, 40, 80, 160) was good [10]. The results for the spherical wave converge (quadratically) to the exact solution given by Eq. 19 [10].

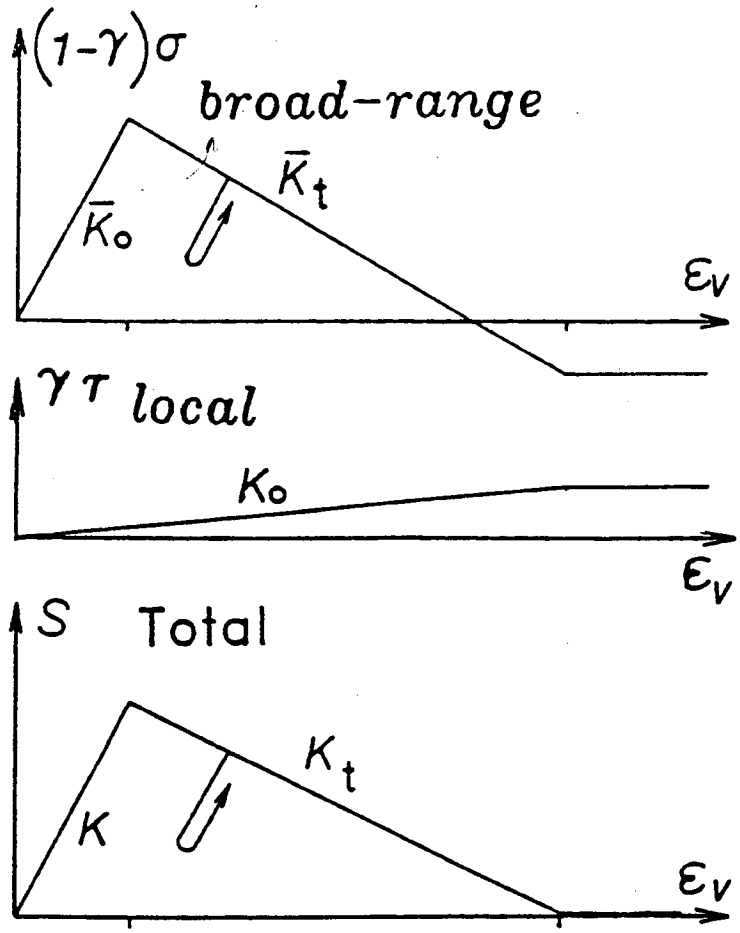

Fig. 9 Local and nonlocal stress strains relations assumed in examples

Subsequently, the problem was solved [10] for a nonlocal continuum ($\varepsilon_0 = 1$, $\varepsilon_f = 5$) with characteristic length $\ell = L/10 = 9 = \text{constant}$. The results for progressively refined meshes (N = 10, 20, 40, 80, 160) are shown in Figs. 7 and 8. For comparison, the solution was also run for a local continuum ($\ell = h = L/N = \text{variable}$) having the same stress-strain relation with stress-softening.

The local and nonlocal results are compared in each figure. It is seen (Fig. 7-8) that the nonlocal solutions with strain-softening (right colums) converge well with increasing N. On the other hand, the corresponding local solutions (left columns) do not converge at all.

While an exact solution for a uniaxial planar wave in local strain-softening material has previously been found [30] and the corresponding finite element solutions were shown to converge to it, for the present case no exact local solution with strain-softening has been found. The behavior of the local solutions is quite interesting. Similar to the exact solution for the planar wave, a strain-softening zone of finite size is apparently not obtained for the local material, and strain-softening appears to localize into singular points on the x-axis (the spikes in Figs. 7-8, left columns). These singular points begin to appear, as expected, when the strain at the wavefront grows to reach the strain-softening region, which cannot be closer than 0.3L from the outer surface, as already mentioned. However, in contrast to the planar wave, there is not only one singular point but many, and they appear at different locations for different N (i.e., different with refinements). The impression is that of chaos (reminiscent of the situation in turbulence). The reason for the appearance of a sequence of strain-softening points (the spikes in Figs. 7-8, left columns) is that part of the strain step at the wavefront is transmitted across the point of strain-softening before the stress is reduced to zero. This part of the wave which has crept through represents again an elastic strain wave with a step front, which then grows as the wavefront propagates further until the elastic limit ε_p is reached again. Then the situation repeats itself.

To sum up, the numerical results for the spherical waves [10], as well as the result for planar waves [1], show that the imbricate nonlocal continuum is a mathematiclaly sound model for strain-softening.

5. Constitutive Relations for Strain-Softening

In the analysis of many practical situation, including all fracture tests, the principal stress direction in the fracture process zone remains constant during fracturing. Triaxial strain-softening can then be introduced in the form of Eqs. 1 and 2. However, for some situations, especially in dynamics, it is necessary to describe progressive formation of fracture during which the principal stress directions rotate. In such a case, Eqs. 1-2 are inadequate. A satisfactory formulation can be obtained with an analog of the slip theory of plasticity [35, 36], which was called the microplane model [6, 25, 29]. In this model it is assumed that the strain on a plane of any inclination within the macroscopic smoothing continuum consists of the resolved components of one and the same macroscopic strain tensor ε_{ij}. Using the condition of equal energy dissipation when calculated in terms of the stresses and strains on all such planes and in terms of the macroscopic

stress and strain tensors, one may obtain [6, 25, 29, 32, 33] the stress-strain relation

$$d\sigma_{ij} = D^c_{ijkm}\, d\,\epsilon_{ij} \tag{23}$$

in which

$$D^c_{ijkm} = \int_0^{2\pi} \int_0^{\pi/2} n_i n_j n_k n_m\, F'(e_n)\, \sin\phi\, d\theta d\phi \tag{24}$$

This equation superimposes contributions to inelastic stress relaxations from planes of all directions within the material, defined by spherical coordinates θ and ϕ; n_i are the direction cosines for all such directions, and $F(e_n)$ is a function characterizing the constitutive properties and representing the stress-strain relation for one particular microplane within the material; $e_n = n_i\, n_j\, \epsilon_{ij}$ = normal strain on a plane with direction cosines n_i. The integral in Eq. 24 must be evaluated numerically. Efficient numerical integration formulas for integration as the surface of a sphere are give by Stroud [34], and some further formulas which are superior in certain situations are given in Ref. 32. It has been demonstrated that the microplane model allows description of tensile strain-softening under general stress or strain histories and always leads to a reduction of stress to zero at sufficiently large tensile strain [32, 33].

6. SIZE EFFECT LAW AND ITS GENERALIZATION

From the practical viewpoint, the principal difference of a nonlocal continuum model (and the special case of crack band model) from the usual local finite element models consists in the size effect.

The structural size effect, a salient aspect of fracture mechanics, is observed when geometrically similar structures of different characterististic dimensions d are compared. It can be described in terms of the nominal stress at failure, defined as $\sigma_N = P/bd$ where P = load at failure (maximum load) and b = structure thickness. While according to the strength or yield criteria used in plastic limit design or elastic allowable stress design, σ_N is independent of structure size d, in fracture mechanics σ_N decreases as the structure size increases. This is because fracture mechanics is based on energy criteria for failure.

Introducing an approximate but apparently quite reasonable hypothesis that the energy release caused by fracture is a function of both the fracture length and the area traversed by the fracture process zone, Bažant showed [37] by dimensional analysis and similitude arguments that, for geometrically similar structures or specimens,

$$\sigma_N = Bf'_t\left(1 + \frac{d}{\lambda_0 d_a}\right)^{-1/2} \tag{26}$$

in which f'_t is the direct tensile strength of concrete, d_a is the maximum aggregate size, and d, λ_0 are empirical parameters characterizing the shape of the structure or specimen. According to this size effect law, the plot of log σ_N vs. log (d/d_a) represents a gradual transition from the strength criterion (i.e., σ_N proportional to strength f'_t) to the failure criterion of

the classical, linear elastic fracture mechanics (i.e., σ_N proportional to $d^{-1/2}$). This size effect law is verified, within the limits of inevitable statistical scatter, by all available Mode I fracture tests of concrete and mortar. Moreover, this size effect law has also been shown applicable to the diagonal shear failure of longitudinally reinforced beams without stirrups [38], and is probably applicable to all the so-called brittle failures of reinforced concrete structures.

When the usual, local finite element codes are applied to similar structures with similar meshes, the results exhibit no size effect. On the other hand, when the nonlocal model (or the special case of crack band model) is used, the results conform to the size effect law in Eq. 26, as experience indicates.

Finally, it may be interesting to note that the size effect law in Eq. 26 applies not only to cleavage (Mode I) fractures but also to shear (Mode II) fractures.

The size effect law in Eq. 26 was originally derived by dimensional analysis and similitude arguments from the following fundamental hypothesis:

The total potential energy release W caused by fracture in a given structure is a function of both:

1. The length of the fracture a; and

2. The area of the cracked zone, $nd_a a$.

n is a material constant characterizing the effective width of the micro-cracking zone at the fracture front, and d_a is the maximum aggregate size. The original derivation [37], which used the nondimensional variables $\alpha_1 = a/d$ and $\alpha_2 = nd_a a/d^2$, tacitly implied one further hypothesis, namely that W as a function of the cracked zone area can be linearized. This is because otherwise the functions α_1 and α_2 used in Ref. [37] would not be size-independent as parameter α_2 depends on the relative size d_a/d when a/d is constant. This fact, as well as the need for the additional linearization assumption, was independently discovered by J. Planas and M. Elices [38].

We will now show a different derivation of the size effect law which involves linearization only as an asymptotic approximation that is always admissible, and which at the same time shows a more general form for the size effect law. Instead of the aforementioned nondimensional variables α_1 and α_2, we now choose as nondimensional variables

$$\theta_1 = \frac{a}{d}, \quad \theta_2 = \frac{nd_a a}{ad} = \frac{nd_a}{d} \tag{26}$$

We consider geometrically similar structures of different sizes d, which are characterized by a constant ratio a/d. Thus, parameter θ_1 is size-independent, while parameter θ_2 characterizes the size. As before [37], the potential energy release W of any structure may always be written in the form

$$W = \frac{1}{2E_c} \left(\frac{P}{bd}\right)^2 bd^2 F(\theta_1, \theta_2, \xi_i) \tag{27}$$

in which E_c is the Young's elastic modulus, b is the thickness of the structure, P is the maximum load (i.e., the failure load in a load-controlled test), F is a certain funtion of nondimensional parameters, and ξ_i are parameters characterizing the structure shape (geometry) which are constant when geometrically similar structures are considered. The nominal stress at failure may be defined as $\sigma_N = P/bd$. Then, substituting $P = \sigma_N bd$ and Eq. 27 into the well known fracture equilibrium relation

$$\frac{\partial W}{\partial a} = G_f b \tag{28}$$

where G_f is the fracture energy, we obtain

$$\frac{1}{2E_c} \frac{\sigma_N^2 b^2 d^2}{b} \frac{\partial F}{\partial \theta_1} \frac{1}{d} = G_b b \tag{29}$$

for which

$$\sigma_N = \frac{\sqrt{2G_f E_c}}{\sqrt{\frac{\partial F(\theta_1, \theta_2, \xi_i)}{\partial \theta_1} d}} \tag{31}$$

In this formulation, the fracture energy itself is considered to be size-independent, being regarded as the final value of the R-curve. According to the blunt crack band theory, $G_f = w_c \left(1-E_c/E_t\right) f_t'^2/2E_c$, in which f'_t = direct tensile strength and E_t = mean slope of the strain-softening portion of the stress-strain diagram = strain-softening modulus. After substitution for G_f, Eq. 31 becomes

$$\sigma_N^2 = \frac{w_c\left(1 - \frac{E_c}{E_t}\right) f_t'^2}{\frac{\partial F(\theta_1, \theta_2, \xi_i)}{\partial \theta_1} d} \tag{31}$$

We may now choose the state $\theta_2 = 0$, which corresponds to an infinitely large structure, $d/d_a \to \infty$, as the reference state, and introduce the following Taylor series expansion about this reference state, which must be possible since W is a smooth funtion of θ_2;

$$\frac{\partial F(\theta_1, \theta_2, \xi_i)}{\partial \theta_1} = F_1(\theta_1, \xi_i) + F_2(\theta_1, \xi_i)\theta_2 + F_3(\theta_1, \xi_i)\theta_2^2 + F_3(\theta_1, \xi_i)\theta_2^3 + \ldots \tag{32}$$

in which

$$F_1(\theta_1, \xi_i) = \left[\frac{\partial F}{\partial \theta_1}\right]_{\theta_2=0}, \quad F_2(\theta_1, \xi_i) = \left[\frac{\partial^2 F}{\partial \theta_1^2}\right]_{\theta_2=0},$$

$$F_3(\theta_1, \xi_i) = \frac{1}{2!}\left[\frac{\partial^3 F}{\partial \theta_i^3}\right]_{\theta_2=0}, \quad F_4(\theta_1, \xi_i) = \frac{1}{3!}\left[\frac{\partial^4 F}{\partial \theta_1^4}\right]_{\theta_2=0} \tag{33}$$

Now, introducing this expansion into Eq. 31 we obtain, after some rearrangements

$$\sigma_N = Bf_t' \left[1 + \frac{d}{\lambda_0 d_a} + \lambda_1 \frac{d_a}{d} + \lambda_2 \left(\frac{d_a}{d}\right)^2 + \lambda_3 \left(\frac{d_a}{d}\right)^3 + \ldots\right]^{-1/2} \tag{36}$$

in which we introduced the notations

$$B = \frac{w_c''}{F_2 n d_a}\left(1 - \frac{E_c}{E_t}\right), \quad \lambda_0 = \frac{nF_2}{F_1}, \quad \lambda_1 = n\left(\frac{F_3}{F_2}\right), \quad \lambda_2 = n\left(\frac{F_4}{F_2}\right)^{1/2}, \quad \lambda_3 = n\left(\frac{F_5}{F_2}\right)^{1/3} \tag{35}$$

Here B, λ_0, λ_1, λ_2, ... are empirical constants to be determined by fitting test data for failure loads of geometrically similar specimens of different sizes. These constants are different for each different geometry. (Note that the derivatives in Eq. 33 are size-independent, since they are evaluated at a fixed value of the size parameter θ_2.)

Let us now check the limiting cases. For a very large structure, $d/d_a \to \infty$, the second term in the bracket of Eq. 34 dominates and we have

$$\sigma_N = Bf_t' \frac{\sqrt{\lambda_0 d_a}}{\sqrt{d}} = \frac{\text{const.}}{\sqrt{d}} \tag{37}$$

This coincides with the well known size-dependence of all solutions according to linear elastic fracture mechanics. The size of the smallest possible structure is a certain fixed multiple of the maximum aggregate size, say $d = 3d_a = nd_a$, and substituting $d/d_a = 3$ into Eq. 35, we find that the nominal stress at failure is

$$\sigma_N = B_0 f_t' \tag{38}$$

where B_0 is a constant. This is the failure criterion used in limit analysis (plasticity) as well as in the allowable stress design. This criterion, as is well known, involves no size effect.

For a structure which is not too small, the first two terms of the bracket in Eq. 34 dominate over the remaining terms, and neglecting these remaining terms we obtain Eq. 25, the originally derived size-effect law. Analyses of available test data so far indicate that this form is adequate for practical applications throughout the entire range of sizes. To be able to

identify coefficients λ_1,.from test data, one would need a test series with an extremely large range of sizes and with an extremely small statistical scatter.

Eq. 25 has, of course, the advantage that its parameters can be identified from test data by linear regression, whereas for Eq. 34 with more than the first two terms in the bracket a nonlinear optimization subroutine must be used to evaluate the test results.

7. CONCLUSION

The concept of imbricate nonlocal continuum, along with strain-softening stess-strain relations, allows a mathematically consistent and realistic description of progressive distributed cracking the concrete structures. When fine resolution inside the strain-softening zone is not needed, this approach reduces to the crack band theory. Examples of one-dimensional planar and spherical waves demonstrate that stable strain-softening regions of finite size can modeled. Strain-softening constitutive relations can be obtained from the microplane model. The results of nonlocal finite element model conform to the size effect laws.

Acknowledgement. - Partial financial support under AFOSR Grant No. 83-0009 to Northwestern University is gratefully acknowledged. Mary Hill is thanked for her exemplary secretarial assistance.

REFERENCES

[1] BAŽANT Z.P., CHANG T.P., BELYTSCHKO T.B., Continuum Theory for Strain Softening, Report No. 83-11/428c, Center for Concrete and Geomaterials, Northwestern University, Evanston, Illinois, Nov. 1983; also Journ. Eng. Mech. ASCE, Vol. III, Dec. 1984, pp. 1666-1692

[2] BAŽANT Z.P., Imbricate Continuum and Its Variational Derivation, Report No. 83-11/428i, Center for Concrete and Geomaterials, Northwestern University, Evanston, Illinois, Nov. 1983; also Journ. Eng. Mech. ASCE, Vol. III, Dec. 1984, pp. 1693-1712.

[3] BAŽANT Z.P., Instability, Ductility and Size Effect in Strain-Softening Concrete; Journal of the Engineering Mechanics Division ASCE, Vol. 102, Apr. 1976, pp. 331 - 344; Discussions Vol. 103, pp. 357 - 358, 775 - 777, Vol. 104, pp. 501 - 502.

[4] BAŽANT Z.P., Crack Band Model for Fracture of Geomaterials, Proc. 4th Intern. Conf. on Numerical Methods in Geomechanics, held in Edmonton, Alberta, Canada, June 1982, ed. by Z. Eisenstein, Vol. 3, pp. 1137-1152.

[5] BAŽANT Z.P., OH, B.H., Crack Band Theory for Fracture of Concrete, Materials and Structures (RILEM, Paris), Vol. 16, 1983, pp. 155-177.

[6] BAŽANT Z.P., OH B.H., Microplane Model for Fracture Analysis of Concrete Structures, Proc. Symp. on the Interaction of Nonnuclear Munitions with Structures, U.S. Air Force Academy, Colorado Springs, May 1983, pp. 49 - 55.

[7] BAŽANT Z.P., CEDOLIN L., Blunt Crack Band Propagation in Finite Element Analysis, Journal of the Engineering Mechanics Division, ASCE, Vol. 105, No. EM2, April 1979, pp. 297-315.

[8] BAŻANT Z.P., CEDOLIN L., Fracture Mechanics of Reinforced Concrete, Journal of the Engineering Mechanics Division, ASCE, Vol. 106, No. EM6, Proc. Paper 15917, December 1980, pp. 1287 - 1306; with Discussion and Closure in Vol. 108, 1982, EM., pp. 464 - 371.

[9] BAŻANT Z.P., CEDOLIN L., Finite Element Modeling of Crack Band Propagation, Journal of Structural Engineering, ASCE, Vol. 109, No. ST2, Feb. 1983, pp. 69 - 92.

[10] BELYTSCHKO T.B., BAŻANT Z.P., HYUN, V.V., and CHANG, T.P., "Strain-Softening Materials and Finite Element Solutions", submitted to Computers and Structures.

[11] HILLERBORG A., MODÉER M., PETERSSON P.E., Analysis of Crack Formation and Crack Growth in Concrete by Means of Fracture Mechanics and Finite Elements, Cement and Concrete Research, Vol. 6, 1976, pp. 773 - 782.

[12] KRÖNER E., Elasticity Theory of Materials with Long-Range Cohesive Forces, Int. J. Solids Structures, Vol. 3, 1967, pp. 731 - 742.

[13] KRÖNER E., Interrelations Between Various Branches of Continuum Mechanics, Mechanics of Generalized Continua, ed. by E. Kröner, Springer-Verlag, 1968, pp. 330 - 340.

[14] KRUMHANSL J.A., Some Considerations of the Relation Between Solid State Physics and Generalized Continuum Mechanics, Mechanics of Generalized Continua, ed. by E. Kroner, Springer-Verlag, 1968, pp. 298 - 311.

[15] KUNIN I.A., The Theory of Elastic Media With Microstructure and the Theory of Dislocations, Mechanics of Generalized Continua, ed. by E. Kröner, Springer-Verlag, 1968, pp. 321 - 328.

[16] LEVIN V.M., The Relation Between Mathematical Expectation of Stress and Strain Tensors in Elastic Microheterogeneous Media: Prikladnaya Matematika i Mekhanika, Vol. 35, 1971, pp. 694 - 701 (in Russian).

[17] ERINGEN A.C., EDELEN D.G.B., On Nonlocal Elasticity, Int. J. Engng. Science, Vol. 10, 1972, pp. 233 - 248.

[18] ERINGEN A.C., ARI N., Nonlocal Stress Field at Griffith Crack, Cryst. Latt. Def. and Amorph. Mat., Vol. 10, 1983, pp. 33 - 38.

[19] ASCE State-of-the-Art Report on Finite Element Analysis of Reinforced Concrete, prepared by a Task Committee chaired by A. Nilson, Am. Soc. of Civil Engrs., New York, 1982.

[20] WITTMANN F.H. (Editor), Fracture Mechanics of Concrete, Elsevier, Netherlands, 1983.

[21] PETERSSON E., Fracture Energy of Concrete: Method of Determination, Cement and Concrete Research, Vol. 10, 1980, pp. 78 - 89, and Fracture Energy of Concrete: Practical Performance and Experimental Results, Cement and Concrete Research, Vol. 10, 1980, pp. 91 - 101.

[22] PETERSSON P.C., Crack Growth and Development of Fracture Zones in Plain Concrete and Similar Materials, Doctoral Dissertation, Lund Institute of Technology, Lund, Sweden, Dec. 1981.

[23] EVANS R.H., MARATHE M.S., Microcracking and Stress-Strain Curves for Concrete in Tension, Materials and Structures (RILEM, Paris), No. 1, Jan. - Feb., 1968, pp. 61 - 64.

[24] HEILMANN H.G., HILDSDORF H.K., FINSTERWALDER K., Festigkeit und Verformung von Beton unter Zugspanungen: Deutscher Ausschuss für Stahlbeton, Heft 203, W. Ernst & Sohn, West Berlin, 1969.

[25] BAŽANT Z.P., Fracture in Concrete and Reinforced Concrete, Chapter 13 in Mechanics of Geomaterials: Rocks, Concretes, Soils, John Wiley & Sons, London, 1985 (Proc. of IUTAM W. Prager Symposium held at Northwestern University in Sept. 1983).

[26] RASHID Y.R., Analysis of Prestressed Concrete Pressure Vessels, Nuclear Engng. and Design, Vol. 7, No. 4, April 1968, pp. 334 - 344.

[27] REINHARDT H.W., CORNELISSEN E., Post-Peak Cyclic Behavior of Concrete in Uniaxial Tension and Alternating Tensile and Compressive Loading, Cement and Concrete Research, Vol. 14, 1984, pp. 263 - 270.

[28] RÜSCH H., HILSDORF H., Deformation Characteristics of Concrete Under Axial Tension, Vorunterschungen, Bericht Nr. 44, Munich, May 1963.

[29] BAŽANT Z.P., Mechanics of Fracture and Progressive Cracking in Concrete Structures, Chap. 1 in Fracture Mechanics Applied to Concrete Structures, ed. by G.C. Sih, Martinus Nijhoff Publishers B.V., The Hague, Netherlands, 1985.

[30] BAŽANT Z.P., and BELYTSCHKO,T.B., "Wave Propagation in a Strain-Softening Bar: Exact Solution", J. of Engineering Mechanics ASCE, Vol. 111, No. 3, March 1985.

[31] ACHENBACH J.D., "Wave Propagation in Elastic Solids", North Holland Publ. Co., Amsterdam 1973.

[32] BAŽANT Z.P., and OH, B.H., "Microplane Model for Progressive Fracture of Concrete and Rock", J. of Engineering Mechanics ASCE, Vol. 111, 1985.

[33] BAŽANT Z.P., and GAMBAROVA R.G., "Crack Shear in Concrete: Crack Band Microplane Model", J. of Engineering Mechanics ASCE, Vol. 110, Sept. 1984, pp. 2015 - 2035.

[34] STROUD A.H., Approximate Calculation of Multiple Integrals, Prentice Hall, Englewood Cliffs 1971, pp. 296 - 302.

[35] TAYLOR G.I., Plastic Strain in Metals; Journal of the Institution of Metals (London), Vol. 62, 1938, pp. 307 - 324.

[36] BATDORF S.B., and BUDIANSKI B., "A Mathematical Theory of Plasticity Based on the Concept of Slip, NACA Technical Note TN 1871, Apr. 1949.

[37] BAŽANT Z.P., "Size Effect in Blunt Fracture: Concrete, Rock, Metal", J. of Engineering Mechanics ASCE, Vol. 110, Apr. 1984, pp. 518 - 535.

[38] ERINGEN A.C., and ARI N. "Nonlocal Stress Field at Griffith Crack," Cryst. Latt. Def. and Amorph. Mat., Vol. 10, 1983, pp. 33 - 38.

[39] PLANAS J., and ELICES M., Private Communication to Z.P. Bažant, Department of Material Science, ETS Universidad Politecnica de Madrid, Spain, March 1985.